Computers and Structures 158 (2015) 346–354

Contents lists available at ScienceDirect

Computers and Structures

journal homepage: www.elsevier.com/locate/compstruc

Transient solution of 3D free surface flows using large time steps

Soyoung You, Klaus-Jürgen Bathe *

Department of Mechanical Engineering, Massachusetts Institute of Technology, 77 Massachusetts Avenue, Cambridge, MA 02139-4307, USA

ARTICLE INFO

Article history:
Received 20 March 2015
Accepted 9 June 2015

Keywords:
Finite elements
ALE
FCBI scheme
Sloshing
Incompressible flows
Mass conservation

ABSTRACT

This paper presents an Arbitrary Lagrangian Eulerian (ALE) formulation derived from the Reynolds transport theorem to accurately solve certain problems of three-dimensional unsteady Newtonian flows with free surfaces. The analysis problems addressed are those without breaking waves or waves spilling over obstructions. The proposed method conserves mass very accurately and obtains stable and accurate results with large time steps, and even when using rather coarse meshes. The continuum mechanics equations are formulated and the three-dimensional Navier–Stokes equations are solved using a 'flow condition based interpolation' (FCBI) scheme for a tetrahedral finite element using finite volume concepts. Various example solutions are given to indicate the effectiveness of the solution schemes.

1. Introduction

Free surface fluid flow analyses solve problems with continuously moving fluid domains. Many industries require free surface solutions, such as vehicle dynamics and earthquake engineering. If free surfaces are not correctly calculated and designed for, the dynamic system may be affected with possible dangerous consequences, for example, an instability may arise due to the fluid motion in large fuel tanks.

Because of the importance of correct free surface solutions, many researchers have attempted to develop methods to calculate incompressible free surface flows in various fields, see for example Refs. [1–10] and the references therein. The Volume of Fluid (VOF) method is a well-known scheme for an Eulerian approach and uses density functions. This approach can ensure mass conservation but a serious disadvantage of the method is that it does not accurately capture free surfaces and interfaces especially in the calculation of three-dimensional flow problems. Another widely used free surface flow calculation method is the level set scheme. This method makes it relatively easy to capture a free surface accurately, using a function which has zero value contour on the free surface as an identifier. However, while the method has desirable capabilities to establish free surfaces and interfaces, difficulties arise in conserving the total mass of the fluid. Of course, these two approaches can also be combined to reach a more effective scheme. An important Lagrangian approach for free surface analyses is the Smoothed Particle Hydrodynamics (SPH) method. The SPH scheme is attractive because a simulation does not require a mesh. However, the disadvantages are that artificial constants such as smoothing factors are used and the method may induce spurious oscillations; thus, it can be difficult to find an accurate solution.

In this paper, we develop an improved numerical method that accurately establishes the free surfaces and robustly achieves mass conservation without requiring any *a posteriori* mass conservation treatment. The formulation uses an arbitrary Lagrangian–Eulerian (ALE) method with a special focus on the condition of accurate mass conservation during long-time response.

The finite element method is employed because of its strong mathematical foundation and the possibility to directly evaluate the Jacobians used for the Newton–Raphson iterations [11]. For the effective solution of the three-dimensional fluid flows governed by the Navier–Stokes equations, we develop a weak formulation of the tetrahedral MINI element (slightly modified) with step weighting functions and flow-condition-based interpolations (FCBI) for the trial functions in the convective terms [12–14]. This approach ensures that the inf–sup condition for modeling incompressible response is passed and stability is maintained regarding the convective terms for high Reynolds number flows. The contribution in the paper is the formulation and the specific 3D element given for the free surface flow conditions considered herein.

In the next sections we first present the finite element formulation and then we give illustrative example solutions.

2. Finite element formulation

In this section, we present a finite element ALE formulation for the transient solution of incompressible fluid flows with free

* Corresponding author.
E-mail address: kjb@mit.edu (K.J. Bathe).

http://dx.doi.org/10.1016/j.compstruc.2015.06.011
0045-7949/

surfaces or interfaces. ALE approaches have of course been amply pursued, see e.g. [15–18], but we focus here on using the Reynolds transport theorem in implicit time integration to achieve a formulation that is effective when using large time steps and coarse finite element meshes.

2.1. Governing equations

Considering the complete fluid flow domain, we have the kinematic relation for the free surface

$$(\underline{u} - \underline{u}_m) \cdot \underline{n} = \quad \text{on} \quad S_f \times [0, T] \tag{1}$$

and the mass conservation equation

$$\frac{\partial \rho}{\partial t} + \nabla \cdot \rho \underline{u} = 0 \quad \text{in} \quad V_f \times [0, T] \tag{2}$$

where $\underline{n}$ is the unit normal vector on the free surface S_f (and also used on any fluid domain), V_f denotes the complete fluid domain (see Fig. 1), ρ is the mass density, $\underline{u}$ is the fluid velocity, $\underline{u}_m$ is the velocity of an underlying medium of observation, which in the ALE formulation is the mesh velocity, and T denotes the time span considered. We assume zero surface tension, and while not explicitly noted variables are of course a function of the spatial coordinates $\underline{x}$ and time t.

Eq. (1) is the kinematic relation on the free surface that is included to satisfy the condition of mass conservation and correctly identify the moving free surface. The mass conservation condition for the interior, Eq. (2) looks as used in compressible flows but we use it here for incompressible flows because we know that the density at a fixed point may change in time due to the motion of the free surface through the fixed point.

In the fluid domain, we name Ω the moving control volume and Γ the surface that encloses the control volume. Using the Reynolds transport theorem, the mass conservation equation in a moving control volume is

$$\frac{d}{dt} \int_\Omega \rho \, d\Omega + \int_\Gamma \rho (\underline{u}_c \cdot \underline{n}) d\Gamma = 0 \tag{3}$$

where $\underline{n}$ is here the outward pointing unit normal to Γ, and $\underline{u}_c$ denotes the convective velocity given by

$$\underline{u}_c = \underline{u} - \underline{u}_m \tag{4}$$

Hence we have

$$\int_\Gamma \rho (\underline{u} \cdot \underline{n}) d\Gamma = -\frac{d}{dt} \int_\Omega \rho \, d\Omega + \int_\Gamma \rho (\underline{u}_m \cdot \underline{n}) d\Gamma \tag{5}$$

The momentum equation using the Reynolds transport theorem is

$$\frac{d}{dt} \int_\Omega \rho \underline{u} d\Omega + \int_\Gamma \rho (\underline{u} \underline{u}_c + p\underline{I} - \mu(\nabla \underline{u} + \nabla \underline{u}^T)) \cdot \underline{n} d\Gamma = \int_\Omega \underline{g} \rho d\Omega \tag{6}$$

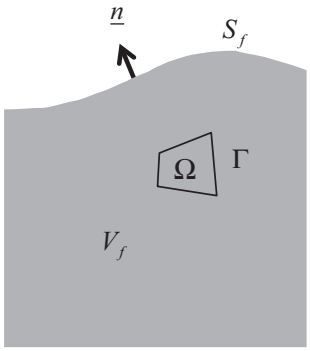

Fig. 1. Complete fluid domain with a free surface.

where $\underline{g}$ is the gravitational acceleration vector. Note that the inertial term accounts for the time rate of change of control volume size. In Eq. (6), we used the stress $\underline{\tau}$ given as

$$\underline{\tau} = \underline{\tau}(\underline{u}, p) = -p\underline{I} + \mu \left\{ \nabla \underline{u} + (\nabla \underline{u})^T \right\} \tag{7}$$

with $\underline{I}$ the identity tensor, p the pressure and μ the viscosity.

The essential boundary conditions are

$$\underline{u} = \underline{u}^S, \quad \underline{x} \in S_v \tag{8}$$

and the natural boundary conditions are

$$\underline{\tau} \cdot \underline{n} = \underline{f}^S, \quad \underline{x} \in S_f \tag{9}$$

where $\underline{u}^S$ is the prescribed velocity on the boundary S_v, $\underline{f}^S$ is the prescribed traction on the boundary S_f, with $S = S_v \cup S_f$ and $S_v \cap S_f = \emptyset$, for the fluid domain, where S denotes the complete boundary.

To solve the momentum and mass conservation equations, Eqs. (5) and (6), we use a Petrov–Galerkin variational formulation in the subspaces U_h, V_h and W_h for the velocities and subspaces P_h and Q_h for the pressure p. The finite element formulation is:

Find $\underline{u} \in U_h, \underline{v} \in V_h$ and $p \in P_h$ such that for all $w \in W_h$ and $q \in Q_h$

$$\frac{d}{dt} \int_\Omega q \rho \, d\Omega + \int_\Gamma q \rho [(\underline{u} - \underline{u}_m) \cdot \underline{n}] d\Gamma = 0 \tag{10}$$

$$\frac{d}{dt} \int_\Omega w[\rho \underline{u}] d\Omega + \int_\Gamma w[\rho \underline{v} \{(\underline{u} - \underline{u}_m) \cdot \underline{n}\}] d\Gamma - \int_\Gamma w[\underline{\tau}(\underline{u}, p) \cdot \underline{n}] d\Gamma = \int_\Omega w[\rho \underline{g}] d\Omega \tag{11}$$

In Eqs. (10) and (11), the trial functions in U_h and in P_h are the conventional finite element interpolations for velocity and pressure, respectively. We select these to satisfy the inf–sup condition of the analysis of incompressible media [19]. The advection term, which is not considered in the Stokes flow assumptions, requires different trial functions in V_h from the functions in U_h. The trial functions in V_h should lead to stability of the method when higher Reynolds number flows are considered and we use the flow-condition-based interpolation approach [12]. Step weight functions are chosen in the spaces W_h and Q_h, to achieve local conservation of momentum and mass, respectively. Hence the formulation is in fact a hybrid between the traditional finite element and finite volume formulations.

2.2. 3D tetrahedral MINI element

The motivation for the development of the tetrahedral element is to be able to generate meshes for complicated 3-D geometries. However, for simple geometries we can use meshes based on hexahedra that are subdivided into tetrahedra. One hexahedron is divided into 6 tetrahedral elements, see Fig. 2.

To establish an FCBI scheme for tetrahedral grids that can be used to solve problems with complex geometries, we develop the MINI tetrahedral element using interpolations to satisfy the inf–sup condition, to give stability in the convective terms, and to satisfy mass and momentum conservation locally [11,12,19].

In a slight modification, instead of using the usual cubic bubble for the MINI element, we use a linear hat function [11].

Fig. 3 shows a MINI element in which the velocity is defined at five nodes, at the local node numbers 1–5, while the pressure is defined at four nodes, at the local node numbers 1–4, in order to satisfy the inf–sup condition [11]. The flux is calculated with interpolated values at the centers of the surfaces of the control volumes for the nodes.

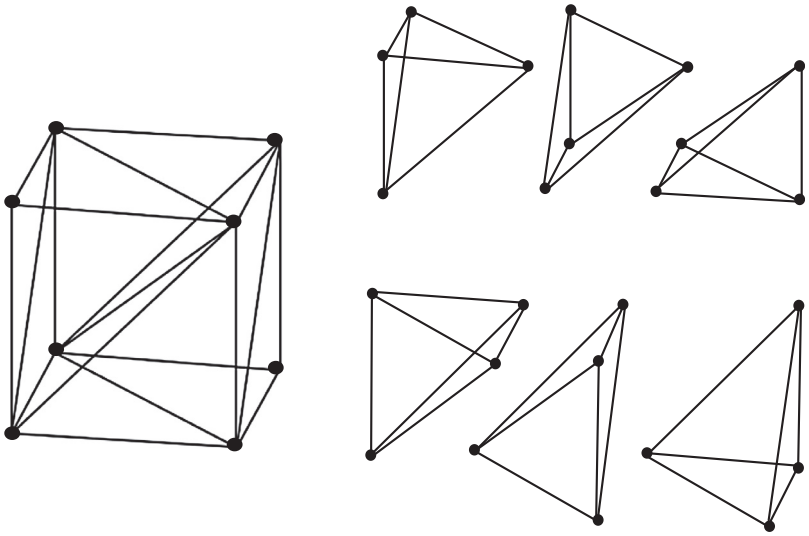

Fig. 2. A hexahedron with its tetrahedral elements.

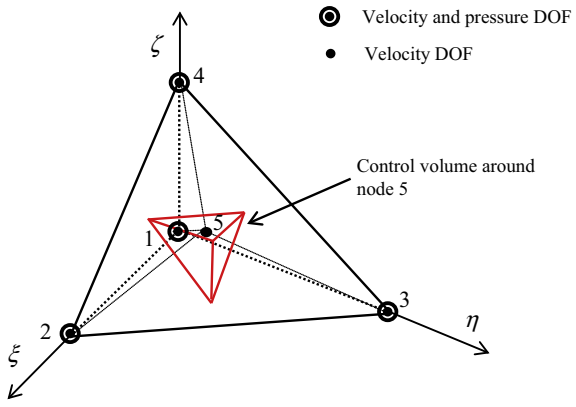

Fig. 3. The 3-D MINI element, showing the control volume for node 5 (used for the momentum equations); the four domains ω_i, $i = 1,\ldots,4$ of the element are: ω_1 = domain with nodes 2, 3, 4 and 5, ω_2 = domain with nodes 1, 3, 4 and 5, ω_3 = domain with nodes 1, 2, 4 and 5, ω_4 = domain with nodes 1, 2, 3 and 5.

The 3-dimensional interpolations for the usual velocities and pressure are given by [11]

$$\underline{u} = h_i^u \hat{\underline{u}}_i \tag{12}$$

$$p = h_i^p \hat{p}_i \tag{13}$$

where $\hat{\underline{u}}_i$ and $\hat{p}_i$ are the nodal velocity and pressure variables, at the local node i, respectively, and we imply summation over i. The unit step weight functions in W_h and Q_h are for the control volumes pertaining to the velocity nodes (for the momentum equations) and the pressure nodes (for the continuity equations), respectively, see Fig. 4.

In order to reach a stable solution scheme for higher Reynolds numbers, $\underline{v}$ in the convection term uses interpolations derived using flow conditions. The scheme is based on using the flow conditions on the faces of the element with an analytical 1-dimensional advection–diffusion equation. In each of the four domains, ω_1, ω_2, ω_3 and ω_4, considering the respective faces that belongs to the region, the velocity is factored into parallel-to-face components $\underline{v}_\parallel$ and normal-to-face components $\underline{v}_\perp$. For the parallel-to-face components, the flow-condition-based interpolation is applied and for the perpendicular components the usual linear interpolation is used

$$\underline{v}_\parallel = h_{i\parallel}^v \underline{v}_{i\parallel} = h_i^v \underline{v}_{i\parallel} \tag{14}$$

$$\underline{v}_\perp = h_{i\perp}^v \underline{v}_{i\perp} = h_i^u \underline{v}_{i\perp} \tag{15}$$

where i is the local node number on the face considered. For the interpolation of the usual velocity and pressure, we use linear interpolations (see Tables 1 and 2).

Of course, for the parallel-to-face components using the 1-dimensional analytical solution of fluid flow (the flow conditions) different schemes could be designed. We use a simple scheme that is as follows for domain 1 using its external surface, see Figs. 5 and 6.

First we interpolate, using the flow conditions at the vertex nodes, the velocities along the edges of the face, see Fig. 5; hence the velocities at points P_{23}, P_{34} and P_{42} are obtained. For each edge (or line referred to below) the interpolation established from the information on the edge, with the convection velocity in the direction of the edge, is applied to both the tangential and perpendicular components of the velocity along the edge. Next, the vertex nodes 2, 3 and 4 and the opposite mid-edge points P_{34}, P_{42} and P_{23} define three lines that intersect at the mid-face point P_{234}. By applying the flow condition interpolation along these three lines in the way as for the edges, see Fig. 6, we obtain three different interpolations of values for each velocity component at the mid-face point which we average.

By solving the 1-D advection–diffusion equation on the element edge, we obtain (see Fig. 5):

$$\underline{v}_\parallel^{P23} = \frac{e^{Re23} - e^{0.5Re23}}{e^{Re23} - 1}\underline{v}_{2\parallel} + \frac{e^{0.5Re23} - 1}{e^{Re23} - 1}\underline{v}_{3\parallel},$$

$$Re23 = \frac{\rho\left[\frac{1}{2}\left(\underline{u}_c^2 + \underline{u}_c^3\right)\cdot\left(\underline{x}_3 - \underline{x}_2\right)\right]}{\mu} \tag{16}$$

where $\underline{x}_3$ and $\underline{x}_2$ are the position vectors of nodes 3 and 2, and $\underline{u}_c^2$ and $\underline{u}_c^3$ are the convective velocities at nodes 2 and 3. The parallel-to-face velocities at the other two mid-edge points are calculated similarly:

$$\underline{v}_\parallel^{P34} = \frac{e^{Re34} - e^{0.5Re34}}{e^{Re34} - 1}\underline{v}_{3\parallel} + \frac{e^{0.5Re34} - 1}{e^{Re34} - 1}\underline{v}_{4\parallel},$$

$$Re34 = \frac{\rho\left[\frac{1}{2}\left(\underline{u}_c^3 + \underline{u}_c^4\right)\cdot\left(\underline{x}_4 - \underline{x}_3\right)\right]}{\mu} \tag{17}$$

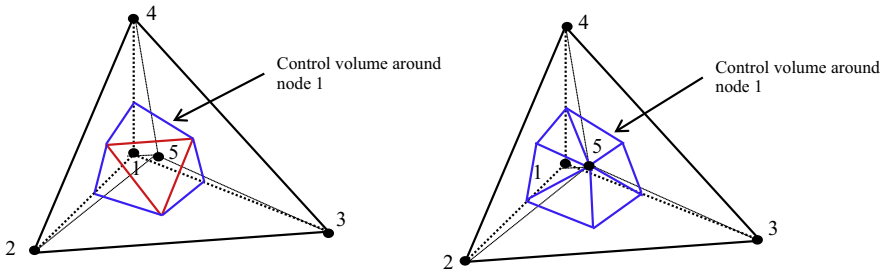

Fig. 4. Typical control volumes and control surfaces: (a) volume for space W_h, the control volume is obtained by triangles formed using mid-face points and mid-edge points and (b) volume for space Q_h, the control volume is obtained by triangles formed using mid-face points, mid-edge points and node 5.

Table 1
Trial functions in U_h for the usual velocity.

Trial function	i	ξ	η	ζ
$h_1^u = 1-\xi-\eta-\zeta-\phi/4$	1	0	0	0
$h_2^u = \xi-\phi/4$	2	1	0	0
$h_3^u = \eta-\phi/4$	3	0	1	0
$h_4^u = \zeta-\phi/4$	4	0	0	1
$h_5^u = \phi$	5	1/4	1/4	1/4

where

$$\phi = \begin{bmatrix} 4(1-\xi-\eta-\zeta) & \text{in region } \omega_1 \\ 4\xi & \text{in region } \omega_2 \\ 4\eta & \text{in region } \omega_3 \\ 4\zeta & \text{in region } \omega_4 \end{bmatrix}.$$

$$\underline{v}_{\parallel}^{P42} = \frac{e^{Re42}-e^{0.5Re42}}{e^{Re42}-1}\underline{v}_{4\parallel} + \frac{e^{0.5Re42}-1}{e^{Re42}-1}\underline{v}_{2\parallel},$$
$$Re42 = \frac{\rho\left[\frac{1}{2}(\underline{u}_c^4+\underline{u}_c^2)\cdot(\underline{x}_2-\underline{x}_4)\right]}{\mu} \tag{18}$$

The values $Re23$, $Re34$ and $Re42$ are the element Reynolds numbers of the convective velocities in the directions of the element edges.

The procedure to find the velocity at the mid-face point P_{234} is to apply the flow condition interpolation along the internal lines

$$\underline{v}_{\parallel}^{2-P34} = \frac{e^{Re234}-e^{0.67Re234}}{e^{Re234}-1}\underline{v}_{\parallel}^{2} + \frac{e^{0.67Re234}-1}{e^{Re234}-1}\underline{v}_{\parallel}^{P34},$$
$$Re234 = \frac{\rho\left[\frac{1}{3}(\underline{u}_c^2+\underline{u}_c^3+\underline{u}_c^4)\cdot\left(\frac{1}{2}(\underline{x}_3+\underline{x}_4)-\underline{x}_2\right)\right]}{\mu} \tag{19}$$

$$\underline{v}_{\parallel}^{3-P42} = \frac{e^{Re342}-e^{0.67Re342}}{e^{Re342}-1}\underline{v}_{\parallel}^{3} + \frac{e^{0.67Re342}-1}{e^{Re342}-1}\underline{v}_{\parallel}^{P42},$$
$$Re342 = \frac{\rho\left[\frac{1}{3}(\underline{u}_c^2+\underline{u}_c^3+\underline{u}_c^4)\cdot\left(\frac{1}{2}(\underline{x}_2+\underline{x}_4)-\underline{x}_3\right)\right]}{\mu} \tag{20}$$

$$\underline{v}_{\parallel}^{4-P23} = \frac{e^{Re423}-e^{0.67Re423}}{e^{Re423}-1}\underline{v}_{\parallel}^{4} + \frac{e^{0.67Re423}-1}{e^{Re423}-1}\underline{v}_{\parallel}^{P23},$$
$$Re423 = \frac{\rho\left[\frac{1}{3}(\underline{u}_c^2+\underline{u}_c^3+\underline{u}_c^4)\cdot\left(\frac{1}{2}(\underline{x}_2+\underline{x}_3)-\underline{x}_4\right)\right]}{\mu} \tag{21}$$

Table 2
Trial functions in P_h for the pressure.

Trial function	i	ξ	η	ζ
$h_1^p = 1-\xi-\eta-\zeta$	1	0	0	0
$h_2^p = \xi$	2	1	0	0
$h_3^p = \eta$	3	0	1	0
$h_4^p = \zeta$	4	0	0	1

where $\underline{v}_{\parallel}^{2-P34}$ is the parallel-to-face velocity at P_{234} using the 1-D flow condition interpolation between points 2 and P_{34}; $\underline{v}_{\parallel}^{3-P42}$ is the parallel-to-face velocity at P_{234} using the 1-D flow condition interpolation between points 3 and P_{42}; and $\underline{v}_{\parallel}^{4-P23}$ is the parallel-to-face velocity at P_{234} using the 1-D flow condition interpolation between points 4 and P_{23}. The final parallel-to-face velocity then assumed at the mid-face point is

$$\underline{v}_{\parallel}^{P234} = \frac{1}{3}\left(\underline{v}_{\parallel}^{2-P34} + \underline{v}_{\parallel}^{3-P42} + \underline{v}_{\parallel}^{4-P23}\right) \tag{22}$$

To complete the interpolation, the vertex nodes, mid-edge points and the mid-face point define six inner triangles (for instance, points 2, P_{23} and P_{234} in Figs. 5 and 6 define one inner triangle). We calculate the velocity values in the inner triangles by linear interpolation of the velocities at the corner points of the triangle.

For the example shown in Fig. 7, the interpolation of $\underline{v}_{\parallel}$ is simply

$$\underline{v}_{\parallel} = (1-r-s)\underline{v}_{2\parallel} + r\underline{v}_{\parallel}^{P23} + s\underline{v}_{\parallel}^{P234} \tag{23}$$

Table 3 lists the interpolation functions, here $f_i^{(j)}$ is the ith interpolating coefficient for the element face that corresponds to region j

$$\tilde{\underline{v}}_{\parallel}^{(j)} = \sum_{i=1,i\neq j}^{4} f_i^{(j)}\underline{v}_{i\parallel} \tag{24}$$

In the table we use linear interpolation between node 5 and the face point reached by projection onto the element face, i.e., $\underline{v}_{\parallel}^{(j)} = (\phi^{(j)})\underline{v}_{5\parallel}^{(j)} + (1-\phi^{(j)})\tilde{\underline{v}}_{\parallel}^{(j)}$, where $\phi^{(j)}$ is the linear bubble function in region j.

For example, considering the inner triangular region shown in Fig. 7, combining Eqs. (16)–(23) gives the values $f_j^{(1)}$, $j = 2, 3, 4$:

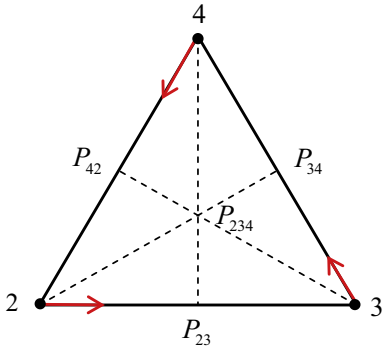

Fig. 5. The 1-D advection–diffusion solution assumption procedure along the element edges.

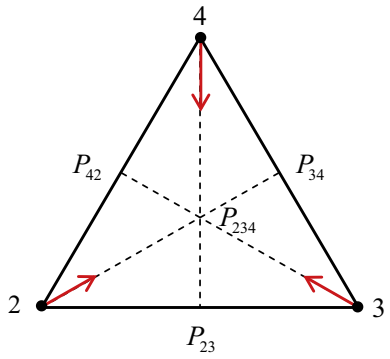

Fig. 6. The 1-D advection–diffusion solution assumption procedure through the element face's center.

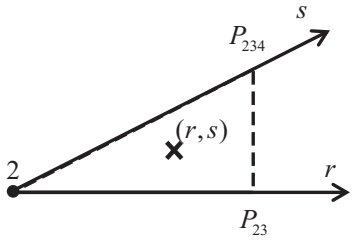

Fig. 7. An inner triangle in an element face that belongs to region 1 in isoparametric coordinates.

trapezoidal rule of time integration. The standard formulae are applied and Newton–Raphson iterations are performed to solve the assembled finite element equations in each time step [11].

2.4. Penalty method for stabilization

Since the problem is highly nonlinear and unsteady, the barycenter node requires a special stabilization. Due to its small volume, by the nature of the tetrahedral geometry, a near singular behavior of the coefficient matrix in the Newton–Raphson iterations can occur. To suppress uncontrolled behavior, a small penalty is applied which increases with the difference in the center node velocity values to the average velocity values of the four corner nodes. The penalty should not have a significant effect on the solution while providing stability [11]. Therefore, Eq. (11) is amended to become

$$\frac{d}{dt}\int_\Omega w[\rho\underline{u}]d\Omega+\int_\Gamma w[\rho\underline{v}\{(\underline{u}-\underline{u}_m)\cdot\underline{n}\}]d\Gamma-\int_\Gamma w[\underline{\tau}(\underline{u},p)\cdot\underline{n}]d\Gamma+\lambda\underline{e}_5^T\left(\underline{u}_5-\frac{1}{4}(\underline{u}_1+\underline{u}_2+\underline{u}_3+\underline{u}_4)\right)=\int_\Omega w[\rho\underline{g}]d\Omega \tag{29}$$

with $\underline{e}_5^T=[0\quad 0\quad 0\quad 0\quad 1]$.

The additional force and the stiffness due to the penalty given by

$$\underline{F}_5^*=\lambda\left(\underline{u}_5-\frac{1}{4}(\underline{u}_1+\underline{u}_2+\underline{u}_3+\underline{u}_4)\right) \tag{30}$$

$$k_{51}^*=-\frac{\lambda}{4},\quad k_{52}^*=-\frac{\lambda}{4},\quad k_{53}^*=-\frac{\lambda}{4},\quad k_{54}^*=-\frac{\lambda}{4},\quad k_{55}^*=\lambda \tag{31}$$

In the solution we use λ to be 10^{-3} times the maximum absolute stiffness value corresponding to the momentum equations of the

$$f_2^{(1)}=\frac{s}{3}\left(\frac{e^{0.67Re234}-1}{e^{Re234}-1}+\frac{e^{Re342}-e^{0.67Re342}}{e^{Re342}-1}\frac{e^{Re42}-e^{0.5Re42}}{e^{Re42}-1}+\frac{e^{0.5Re23}-1}{e^{Re23}-1}\frac{e^{Re423}-e^{0.67Re423}}{e^{Re423}-1}\right)+(1-r-s)+r\left(\frac{e^{Re23}-e^{0.5Re23}}{e^{Re23}-1}\right) \tag{25}$$

$$f_3^{(1)}=\frac{s}{3}\left(\frac{e^{0.67Re342}-1}{e^{Re342}-1}+\frac{e^{Re423}-e^{0.67Re423}}{e^{Re423}-1}\frac{e^{Re23}-e^{0.5Re23}}{e^{Re23}-1}+\frac{e^{0.5Re34}-1}{e^{Re34}-1}\frac{e^{Re234}-e^{0.67Re234}}{e^{Re234}-1}\right)+r\left(\frac{e^{0.5Re23}-1}{e^{Re23}-1}\right) \tag{26}$$

$$f_4^{(1)}=\frac{s}{3}\left(\frac{e^{0.67Re423}-1}{e^{Re423}-1}+\frac{e^{Re234}-e^{0.67Re234}}{e^{Re234}-1}\frac{e^{Re34}-e^{0.5Re34}}{e^{Re34}-1}+\frac{e^{0.5Re42}-1}{e^{Re42}-1}\frac{e^{Re342}-e^{0.67Re342}}{e^{Re342}-1}\right) \tag{27}$$

The scheme of interpolation satisfies the completeness condition, the velocity values are continuous over the element assemblage, the FCBI interpolation values are always positive and at small Reynolds numbers, convergence to the usual interpolation values is reached. The element satisfies the patch test [11]. In addition, the solution scheme shows good stability as we shall demonstrate in Section 3.

2.3. Time rate of change of mass matrix

The unsteady part in Eq. (11) includes a time rate of change of mass which when discretized becomes

$$\frac{d}{dt}\int_\Omega w[\rho\underline{u}]d\Omega\Rightarrow\frac{d}{dt}(\underline{M}\,\hat{\underline{u}})=\frac{d\underline{M}}{dt}\hat{\underline{u}}+\underline{M}\frac{d\hat{\underline{u}}}{dt}=\frac{d\underline{M}}{dt}\hat{\underline{u}}+\underline{M}\,\hat{\underline{a}} \tag{28}$$

where w is the weight function of the momentum equation, which is a unit step function for the FCBI method and $\underline{M}$ is the mass matrix, and $\hat{\underline{u}}$ and $\hat{\underline{a}}$ are the nodal velocity vector and the nodal acceleration vector, respectively. Clearly the inertia is highly dependent on the configuration change of the mesh. For the calculation of this term, we define the mass rate of change and the acceleration using the center node. In our studies we have observed that the solution change due to this very slight penalty is negligible, yet the penalty renders the method quite stable.

3. Numerical examples

In this section we present some experiences that we have obtained with the solution scheme. We emphasize the robustness of the scheme, giving reasonable solutions even when rather large time steps and rather coarse meshes are used.

Table 3
Trial functions in V_h for the velocity component parallel to the element faces.

Trial function	ω_1	ω_2	ω_3	ω_4
$h_{1\|\|}^v$	0	$(1-4\xi)f_1^{(2)}$	$(1-4\eta)f_1^{(3)}$	$(1-4\zeta)f_1^{(4)}$
$h_{2\|\|}^v$	$(4\xi+4\eta+4\zeta-3)f_2^{(1)}$	0	$(1-4\eta)f_2^{(3)}$	$(1-4\zeta)f_2^{(4)}$
$h_{3\|\|}^v$	$(4\xi+4\eta+4\zeta-3)f_3^{(1)}$	$(1-4\xi)f_3^{(2)}$	0	$(1-4\zeta)f_3^{(4)}$
$h_{4\|\|}^v$	$(4\xi+4\eta+4\zeta-3)f_4^{(1)}$	$(1-4\xi)f_4^{(2)}$	$(1-4\eta)f_4^{(3)}$	0
$h_{5\|\|}^v$	$4(1-\xi-\eta-\zeta)$	4ξ	4η	4ζ

In the ALE solutions, a scheme needs to be used to calculate the mesh velocities $\underline{u}_m$ at the nodes of the finite element meshes. For the geometrically simple problems of a fluid in a tank that we consider, we have simply employed the free surface velocities and interpolated the mesh nodal velocities linearly from the free surface to the bottom of the tank.

3.1. 2D cavity driven flow problem

This problem has been used abundantly in the evaluation of numerical solution schemes for fluid flows. Fig. 8 describes the problem.

The solution of this problem does of course not require the ALE formulation and we merely solve the problem to study the solution accuracy obtained with the 3D tetrahedral element. We consider the conditions at Reynolds numbers 1000 and 10,000 with a mesh of 40 hexahedra in each direction x, z. Four layers of hexahedra are used in the y direction in our 3-dimensional solution, merely to check the solution symmetry.

Fig. 9 shows the computed horizontal and vertical velocity profiles at the mid-surfaces at Reynolds numbers 1,000 and 10,000. The results are compared with those given by Ghia et al. [20] and by Kohno and Bathe [14]. Good agreement is seen.

3.2. 2-D sloshing in a rectangular tank

We consider the sloshing of a fluid in a tank that is excited in its longitudinal direction only. The problem is designed to maintain symmetry and experimental data are available, see Fig. 10. The excitation input is given as $x = -0.005(1 - \cos 6.85t)$, where t is time. A mesh of $14 \times 4 \times 14$ hexahedra is used with the time step $\Delta t = 0.03$ s, whereas Ref. [17] used the time step 0.001 s. The fluid material is water with $\mu = 0.001$ kg/(m s) and density, $\rho = 1000$ kg/m^3; also $g = 9.81$ m/s^2 is used. The same fluid material properties and gravitational acceleration are used in Section 3.3.

The 3-D results using this relatively large time step agree well with the experimental and the numerical results given in Ref. [17], see Figs. 11 and 12.

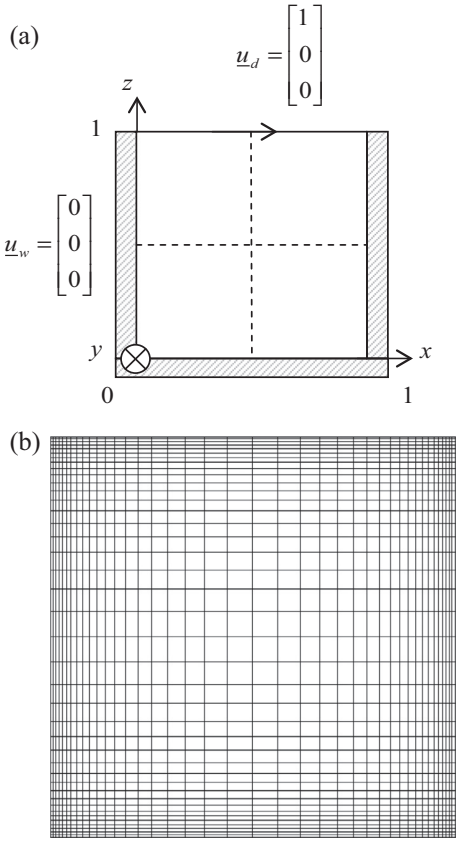

Fig. 8. Square cavity problem (a) definition of problem ($0 \leqslant x \leqslant 1$, $0 \leqslant y \leqslant 1$ and $0 \leqslant z \leqslant 1$) and (b) mesh used; $\underline{u}_d$ = velocity of top moving wall; $\underline{u}_w$ = velocity at three stationary walls.

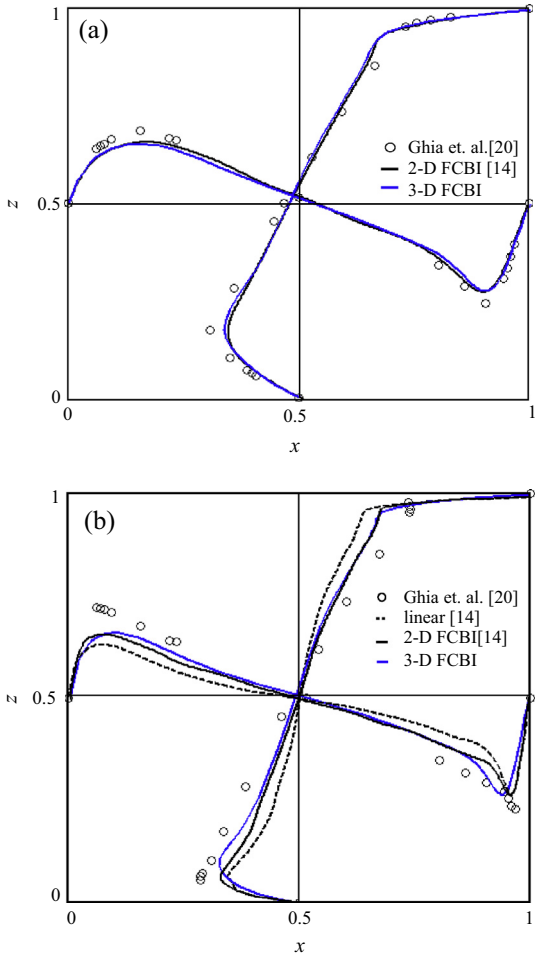

Fig. 9. Vertical velocity profile at the horizontal mid-surface at $z = 0.5$ and horizontal velocity profile at the vertical mid-surface at $x = 0.5$ (a) Re = 1,000 case and (b) Re = 10,000 case.

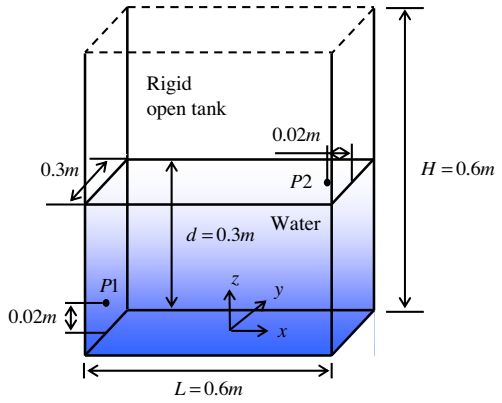

Fig. 10. Problem definition and parameters for liquid sloshing in a rectangular tank.

We note that the computed results with the presented scheme are stable and no special treatment is used to achieve mass conservation (of course symmetry in the y-direction is obtained). The mass conservation error without parameter setting in our solution is 0.0923%, while in Ref. [17] a factor is selected for a good tradeoff between elimination of pressure fluctuation and mass conservation.

Fig. 13 shows the sensitivity of the solution to the time step size used and Fig. 14 gives the results obtained with different meshes. These solutions demonstrate that the scheme is quite robust, but the solution is more sensitive to the mesh size because the free surface is subjected to significant curvature and a sufficiently fine mesh is needed to represent this curvature.

Using the element size and hence mesh size values, given by h

$$h = \sqrt{(\Delta x)^2 + (\Delta z)^2} \tag{32}$$

we define the error in the height calculation at point P2 as

$$E_n = \sqrt{\sum\nolimits_i \left(Z_i^n - Z_i^{ref}\right)^2} \tag{33}$$

where Z_i is the z coordinate of point P2 at time step i and the reference value Z_i^{ref} is calculated with a very fine mesh. The error values are shown in Fig. 15, where it is seen that, for the value considered, 2nd order convergence is obtained.

3.3. 3-D sloshing in a rectangular tank

We consider a 3-D sloshing problem of a fluid excited in a tank with a near-resonance displacement input, see Fig. 16. The purpose of solving this problem is to study the accuracy of the solution scheme in a true three-dimensional sloshing problem.

The open tank is excited with the displacements $d_x = 0.005 \sin\left(0.93\omega_n^{(1)} t\right) \cos 30^\circ$ and $d_y = 0.005 \sin\left(0.93\omega_n^{(1)} t\right) \sin 30^\circ$ in the x and y directions, respectively. The excitation frequency is $0.93\omega_n^{(1)}$ with the natural frequency given as

$$\omega_n^{(1)} = \sqrt{g\pi \tanh(\pi h)} = 4.4957 \text{ s}^{-1} \quad \text{where} \quad h = 0.25 \text{ m} \tag{34}$$

The results obtained in this problem are presented as for the previous problem, and comparisons with the results shown in Ref. [18] are given in Figs. 17–19.

For comparison with the experimental data presented in Ref. [18], we have shifted the simulation results in Fig. 18 and 19 by 0.2 s to take into account the abrupt start of the experimental measurement (evidenced in Fig. 17).

Since this case is a 3-D solution, the 'effective element length' must include the 3rd direction

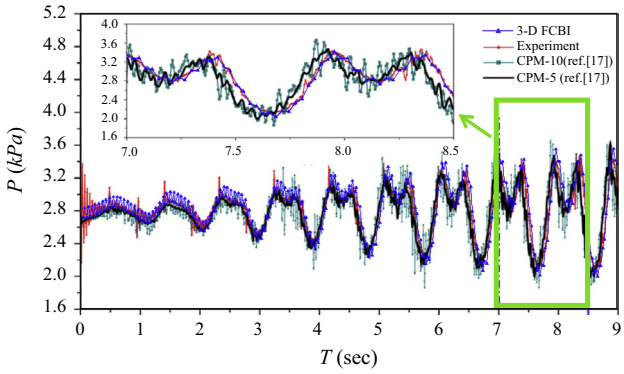

Fig. 12. Time history of pressure at the reference point P1 in Fig. 10.

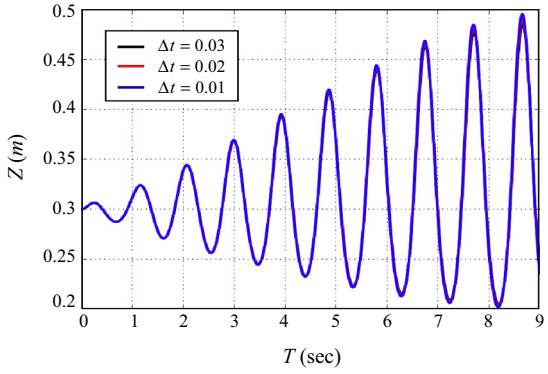

Fig. 13. Time history of z coordinate at point P2 due to different time step sizes.

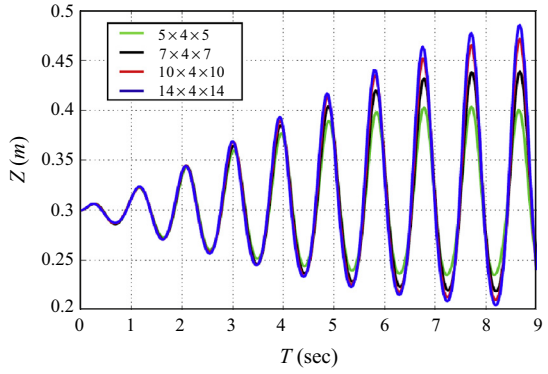

Fig. 14. Time history of z coordinate at point P2 when using different meshes, $\Delta t = 0.03$ s.

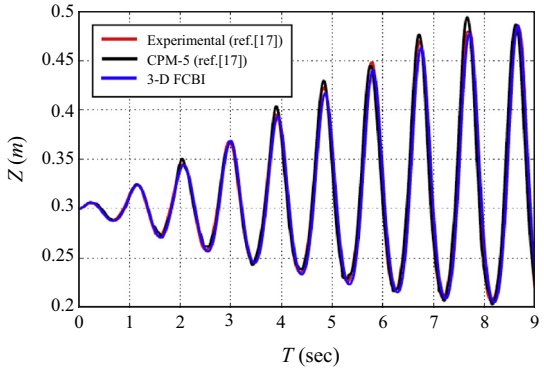

Fig. 11. Time history of height at the reference point P2 in Fig. 10.

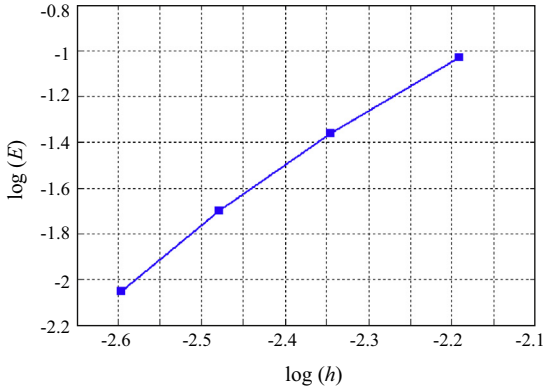

Fig. 15. Convergence of height value at point P2 for problem in Fig. 10; $\Delta t = 0.03$ s.

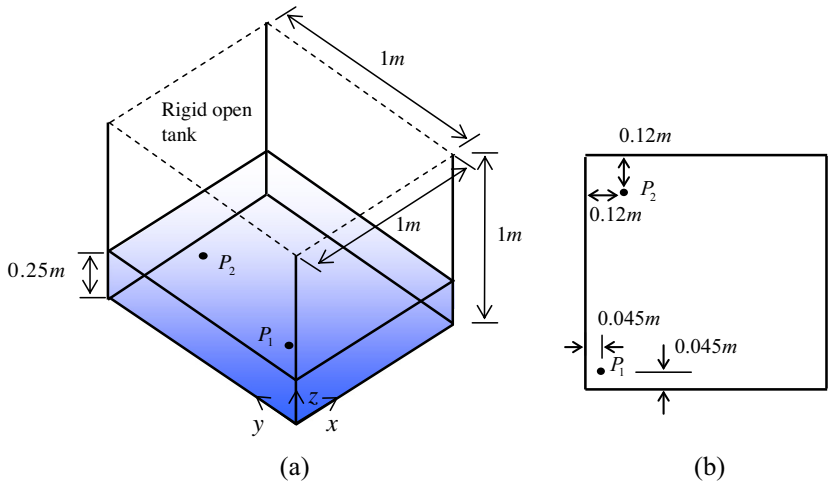

Fig. 16. Definition of the 3-D liquid sloshing problem in a rectangular tank. (a) iso-view of tank and (b) plan-view of tank with location of calculation points.

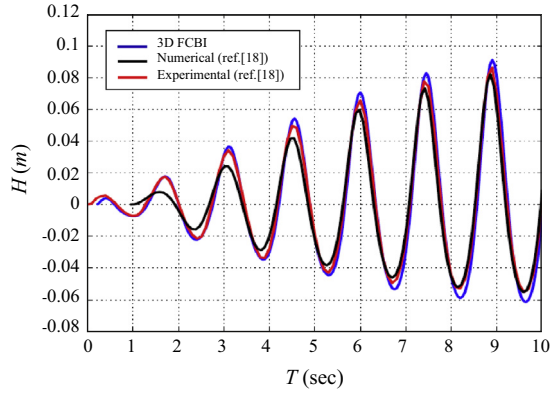

Fig. 17. History of the height of reference point P1; using a $20 \times 20 \times 10$ mesh of hexahedra.

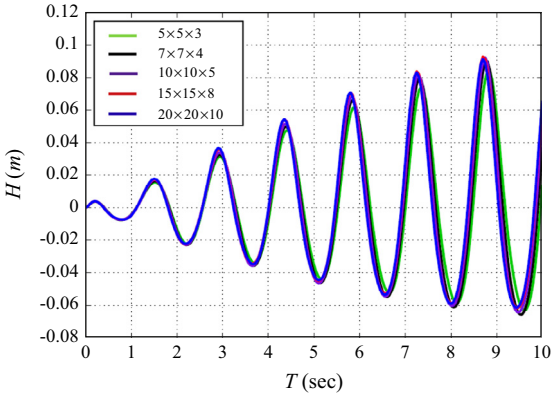

Fig. 19. Time history of height at point P1 using different meshes.

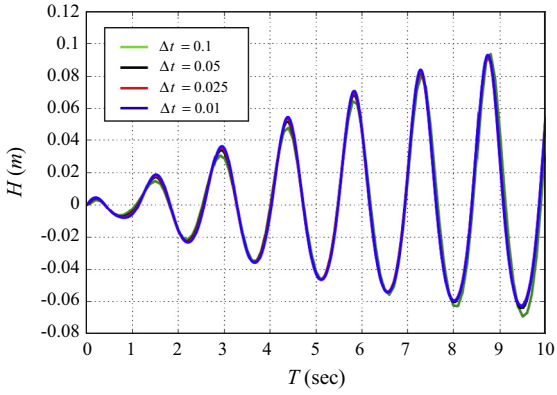

Fig. 18. Time history of height of point P1 due to different time step sizes.

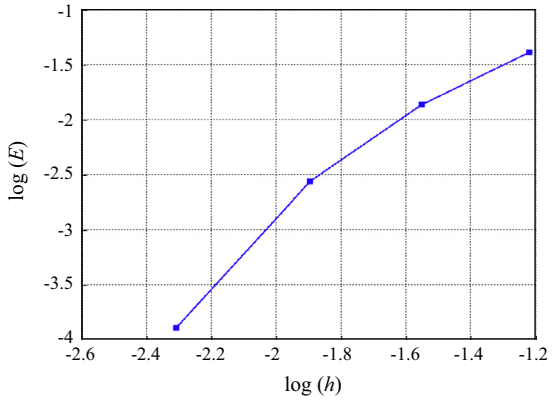

Fig. 20. Convergence of height value at point P1 for problem in Fig. 16; $\Delta t = 0.01$ s.

$$h = \sqrt{\Delta x^2 + \Delta y^2 + \Delta z^2} \tag{35}$$

Fig. 20 shows the convergence obtained with $\Delta t = 0.01$ s as the mesh is being refined. The convergence rate is close to 2nd order convergence.

4. Concluding remarks

Our objective in this paper was to present a solution scheme for the analysis of free surface fluid flows with emphasis on being able to use relatively large time steps and coarse meshes. Many attempts have been made to reach an effective solution scheme for free surface fluid flows but the requirements of stability, accuracy and to locally and globally conserve mass and momentum

have proven it difficult to reach an efficient scheme that is effective in general 3-dimensional solutions.

We use the Reynolds transport theorem in an ALE formulation, an effective finite element formulation for a tetrahedral element and implicit time integration in the proposed solution method. While we have not provided a mathematical analysis of the procedure, the numerical solutions given in the paper indicate that the solution scheme is quite stable and gives good accuracy. Of course, further numerical studies of the scheme would be very valuable and a mathematical analysis would give insight.

However, the solution procedure is clearly only applicable to a certain class of free surface fluid flow problems. Significant additional difficulties arise, for example, when the free surface undergoes very large motions with breaking of waves and fluid leaving a container. Further developments perhaps to reach a hybrid scheme are needed to simulate such fluid flow actions reliably and accurately.

Acknowledgements

We are grateful to the authors of Refs. [17,18] for providing their experimental data with their numerical results. We are also thankful for the partial financial support of this work by a Kwanjeong Fellowship, and Soyoung You thanks Jean-Philippe Péraud for useful comments.

References

[1] Hirt CW, Nichols BD. Volume of fluid (VOF) method for the dynamics of free boundaries. J Comput Phys 1981;39:201–25.
[2] Bathe KJ, Khoshgoftaar M. Finite-element free-surface seepage analysis without mesh iteration. Int J Numer Anal Methods Geomech 1979;3:13–22.
[3] Osher S, Sethian JA. Fronts propagating with curvature-dependent speed: algorithms based on Hamilton–Jacobi formulations. J Comput Phys 1988;79:12–49.
[4] Lopez J, Hernandez J, Gomez P, Faura F. An improved PLIC-VOF method for tracking thin fluid structures in incompressible two-phase flows. J Comput Phys 2005;208:51–74.
[5] Enright D, Fedkiw R, Ferziger J, Mitchell I. A hybrid particle level set method for improved interface capturing. J Comput Phys 2002;183:83–116.
[6] Enright D, Losasso F, Fedkiw R. A fast and accurate semi-Lagrangian particle level set method. Comput Struct 2005;83:479–90.
[7] Grooss J, Hesthaven JS. A level set discontinuous Galerkin method for free surface flows. Comput Methods Appl Mech 2006;195:3406–29.
[8] Bonometti T, Magnaudet J. An interface-capturing method for incompressible two-phase flows. Validation and application to bubble dynamics. Int J Multiphase Flow 2007;33:109–33.
[9] Kees CE, Akkerman I, Farthing MW, Bazilevs Y. A conservative level set method suitable for variable-order approximations and unstructured meshes. J Comput Phys 2011;230:4536–58.
[10] Liu MB, Liu GR. Smoothed particle hydrodynamics (SPH): an overview and recent developments. Arch Comput Methods Eng 2010;17:25–76.
[11] Bathe KJ. Finite element procedures. 2nd ed. Watertown (MA): KJ Bathe; 2014.
[12] Bathe KJ, Zhang H. A flow-condition-based interpolation finite element procedure for incompressible fluid flows. Comput Struct 2002;80:1267–77.
[13] Bathe KJ, Zhang H. Finite element developments for general fluid flows with structural interactions. Int J Numer Methods Eng 2004;60:213–32.
[14] Kohno H, Bathe KJ. A flow condition-based interpolation finite-element procedure for triangular grids. Int J Numer Methods Fluids 2006;51:673–99.
[15] Okamoto T, Kawahara M. Two-dimensional sloshing analysis by Lagrangian finite- element method. Int J Numer Methods Fluids 1990;11:453–77.
[16] Braess H, Wriggers P. Arbitrary Lagrangian Eulerian finite element analysis of free surface flow. Comput Methods Appl Mech 2000;190:95–109.
[17] Koh CG, Luo M, Gao M, Bai W. Modelling of liquid sloshing with constrained floating baffle. Comput Struct 2013;122:270–9.
[18] Wu CH, Chen BF, Hung TK. Hydrodynamic forces induced by transient sloshing in a 3D rectangular tank due to oblique horizontal excitation. Comput Math Appl 2013;65:1163–86.
[19] Bathe KJ. The inf–sup condition and its evaluation for mixed finite element methods. Comput Struct 2001;79:243–52 (971).
[20] Ghia U, Ghia KN, Shin CT. High-Re solutions for incompressible flow using the Navier–Stokes equations and a multigrid method. J Comput Phys 1982;48:387–411.